Norm-1 Regularized Consensus-Based ADMM for Imaging With a Compressive Antenna

Juan Heredia-Juesas, Ali Molaei, Luis Tirado, William Blackwell, and José Á. Martínez-Lorenzo

***Abstract*—This letter presents a novel norm-1-regularized, consensus-based imaging algorithm, based on the alternating direction method of multipliers (ADMM). This algorithm is capable of imaging metallic targets by using a limited amount of data. The distributed capabilities of the algorithm enable a fast imaging convergence. Recently, a compressive reflector antenna (CRA) has been proposed as a way to provide high sensing capacity with a minimum cost and complexity in the hardware architecture. The ADMM algorithm applied to the imaging capabilities of the CRA outperforms current state-of-the-art iterative reconstruction algorithms, such as Nesterov-based methods, in terms of computational cost, enabling the use of the CRA in quasi-real-time, compressive sensing imaging applications.**

***Index Terms*—Consensus alternating direction method of multipliers (ADMM), compressive antenna, norm-1 regularization, real-time imaging.**

I. Introduction

REDUCING the cost of electromagnetic sensing and imaging systems is a necessity before they can be ubiquitously deployed as a part or a large-scale network of sensors. Recently, a single transceiver compressive reflector antenna (CRA) was proposed as a vehicle to enhance the sensing capacity of an active imaging system, which is equivalent to maximizing the information transfer efficiency from the imaging domain and radar system [1], [2]. As a result, the cost and hardware architecture of the imaging system can be drastically reduced [1]. This unique feature of CRAs has triggered its use in a wide variety of applications, which include the following:

1) active imaging of metallic target at millimeter (mm)-wave frequencies [1], [3];
2) passive imaging of the physical temperature of the earth at mm-wave frequencies [4];
3) active imaging of red blood cells at optical frequencies [5].

Manuscript received April 7, 2017; accepted May 29, 2017. Date of publication June 21, 2017; date of current version August 14, 2017. This work was funded by the NSF CAREER program under Award 1653671 and the DHS under Grant 2013-ST-061-ED0001. *(Corresponding author: José Á. Martinez-Lorenzo.)*

J. Heredia-Juesas and J. A. Martínez-Lorenzo are with the Departments of Electrical & Computer Engineering and Mechanical & Industrial Engineering, Northeastern University, Boston, MA 02115 USA (e-mail: j.herediajuesas@neu.edu; jmartinez@coe.neu.edu).

A. Molaei and L. Tirado are with the Department of Electrical and Computer Engineering, Northeastern University, Boston, MA 02115 USA (e-mail: amolaei@coe.neu.edu; tirado.l@husky.neu.edu).

W. Blackwell is with the Lincoln Laboratory, Massachusetts Institute of Technology, Lexington, MA 02139 USA (e-mail: wjb@ll.mit.edu).

Color versions of one or more of the figures in this letter are available online at http://ieeexplore.ieee.org.

Digital Object Identifier 10.1109/LAWP.2017.2718242

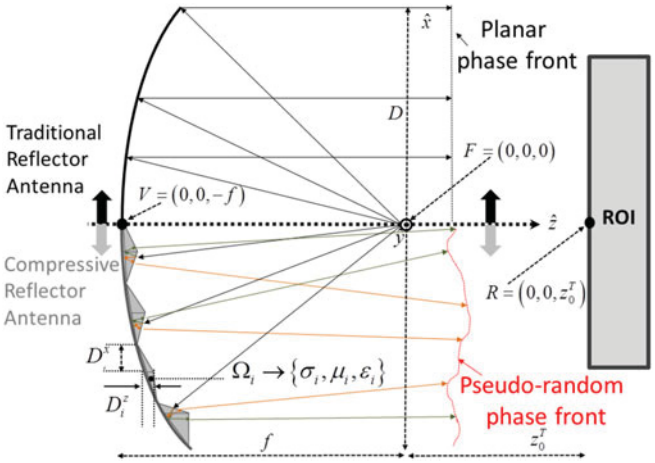

Fig. 1. Two-dimensional cross section of a TRA ($x > 0$), and CRA ($x < 0$), where all the design parameters are described.

CRAs rely on the use of norm-1-regularized iterative compressive sensing (CS) imaging techniques, such as Bayesian CS [6], by enforcing a probabilistic hierarchical prior as a sparsity regularization constraint; FISTA [7], an extension of the classical gradient algorithm; NESTA [8], a robust first-order method that solves basis-pursuit problems; and others [9], but they are slow and computationally very expensive. This can compromise CS use in quasi-real-time imaging applications. In order to overcome these imaging barriers, this letter proposes a new fully parallelizable, consensus-based imaging algorithm, based on the alternating direction method of multipliers (ADMM) formulation.

II. Compressive Reflector Antenna

A. General Description

The concept of operation of the CRA for sensing and imaging applications relies on two basic principles: 1) multidimensional codification, generated by the design of a customized reflector; and 2) compressed sensing, performed on under-sampled measured data.

The CRA is fabricated as described in [1]. Fig. 1 shows a cross section of a reflector, comparing between a traditional reflector antenna (TRA) ($x > 0$) and a CRA, ($x < 0$), by introducing discrete scatterers, Ω_i, on the surface of the reflector. Each scatterer Ω_i is characterized by the electromagnetic parameters: conductivity, permeability, and permittivity, $\{\sigma_i, \mu_i, \epsilon_i\}$, and the scatterer size $\{D_i^x, D_i^y, D_i^z\}$ in $\{\hat{\mathbf{x}}, \hat{\mathbf{y}}, \hat{\mathbf{z}}\}$. CRA and TRA share many geometrical parameters: D, aperture size; f, focal length; and h_o, offset height. These scatterers generate a spatially coded

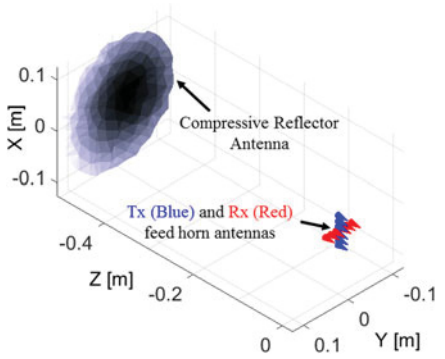

Fig. 2. Geometry of the CRA with the feed horns at the focal plane.

pattern in the near and far fields of the antenna after reflecting the incident field produced by the feeding element. When this coded pattern is changed as a function of time, CS techniques can be used to generate a three-dimensional (3-D) image of an object under test.

B. Computation of Sensing Matrix

Following the example carried out in this letter, the configuration defined in Fig. 2 is selected to generate the coded pattern with N_{Tx} transmitter and N_{Rx} receiver horns, arranged in a cross-shaped configuration around the focal point. Each receiver collects the signal from each transmitter for N_f different frequencies, for a total of $N_m = N_{\mathrm{Tx}} \cdot N_{\mathrm{Rx}} \cdot N_f$ measurements. The image reconstruction domain is performed in N_p pixels, on a region of interest (ROI) located z_0^T meters away from the focal point of the CRA. Under this configuration, the sensing matrix $\mathbf{H} \in \mathbb{C}^{N_m \times N_p}$, computed as described in [10], establishes a linear relationship between the unknown complex vector of reflectivity in each pixel $\mathbf{u} \in \mathbb{C}^{N_p}$, and the measured complex field data $\mathbf{g} \in \mathbb{C}^{N_m}$. This relationship can be expressed in a matrix form as follows:

$$\mathbf{g} = \mathbf{H}\mathbf{u} + \mathbf{w} \tag{1}$$

where $\mathbf{w} \in \mathbb{C}^{N_m}$ represents the noise collected by each receiver antenna, when transmitting with a given transmitter antenna and for a given frequency.

III. ADMM Formulation

Equation (1) may be solved by minimizing the convex function $f(\mathbf{u}) = \|\mathbf{H}\mathbf{u} - \mathbf{g}\|_2^2$ together with the norm-1 regularized $g(\mathbf{u}) = \lambda \|\mathbf{u}\|_1$, in order to obtain a sparse solution. Since we are applying CS, the matrix $\mathbf{H}$ must satisfy the restricted isometry property [2], [11] and a suitable sampling criteria. The minimization of the conjunction of $f(\mathbf{u}) + g(\mathbf{u})$ can be solved via a novel method for optimizing convex functions called the ADMM, [12], [13]. The general representation of an optimization problem through the ADMM takes the following form:

$$\begin{aligned} &\text{minimize } f(\mathbf{u}) + g(\mathbf{v}) \\ &\text{s.t.} \quad \mathbf{P}\mathbf{u} + \mathbf{Q}\mathbf{v} = \mathbf{c} \end{aligned} \tag{2}$$

where f and g are convex, closed, and proper functions over the unknown vectors $\mathbf{u} \in \mathbb{C}^n$ and $\mathbf{v} \in \mathbb{C}^m$. The known matrices $\mathbf{P} \in \mathbb{C}^{p \times n}$ and $\mathbf{Q} \in \mathbb{C}^{p \times m}$, and vector $\mathbf{c} \in \mathbb{C}^p$, are the ones that define the constraint. In order to be able to optimize over f and g separately, the methodology of the ADMM introduces the new variable $\mathbf{v}$, so that both variables $\mathbf{u}$ and $\mathbf{v}$ can be updated in an *alternating direction* fashion. Due to the incorporation of that variable, a constraint needs to be added. Thus, the ADMM problem for solving (1) takes the *lasso* form, and is formulated as follows:

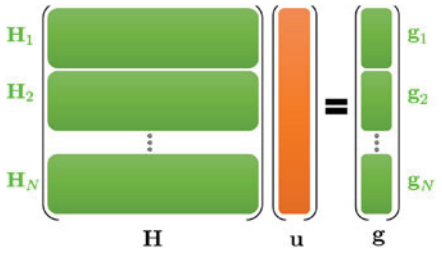

Fig. 3. Division of the system by rows.

$$\begin{aligned} &\text{minimize } \tfrac{1}{2} \|\mathbf{H}\mathbf{u} - \mathbf{g}\|_2^2 + \lambda \|\mathbf{v}\|_1 \\ &\text{s.t.} \quad \mathbf{u} - \mathbf{v} = \mathbf{0} \end{aligned} \tag{3}$$

where $\mathbf{P} = \mathbf{I}$, $\mathbf{Q} = -\mathbf{I}$, and $\mathbf{c} = \mathbf{0}$ enforce that the variables $\mathbf{u}$ and $\mathbf{v}$ are equal. This problem can be solved in a distributed fashion, by splitting the original matrix $\mathbf{H}$ and the vector $\mathbf{g}$ into N submatrices $\mathbf{H}_i$ (by rows) and N subvectors $\mathbf{g}_i$, respectively, as shown in Fig. 3. Additionally, it is possible to define N different variables $\mathbf{u}_i$, so that (3) turns into

$$\begin{aligned} &\text{minimize } \tfrac{1}{2} \sum_{i=1}^{N} \|\mathbf{H}_i \mathbf{u}_i - \mathbf{g}_i\|_2^2 + \lambda \|\mathbf{v}\|_1 \\ &\text{s.t.} \quad \mathbf{u}_i = \mathbf{v}, \quad \forall i = 1, ..., N. \end{aligned} \tag{4}$$

Equation (4) is solved as N different problems. The variable $\mathbf{v}$ works as a *consensus* variable, imposing the agreement between all the variables $\mathbf{u}_i$. See, for example, [14]–[17]. The augmented Lagrangian function for this problem is of the following form:

$$\begin{aligned} L_\rho(\mathbf{u}_i, \mathbf{v}, \mathbf{s}_i) = &\frac{1}{2} \sum_{i=1}^{N} \|\mathbf{H}_i \mathbf{u}_i - \mathbf{g}_i\|_2^2 + \lambda \|\mathbf{v}\|_1 \\ &+ \frac{\rho}{2} \sum_{i=1}^{N} \|\mathbf{u}_i - \mathbf{v} + \mathbf{s}_i\|_2^2 - \frac{\rho}{2} \sum_{i=1}^{N} \|\mathbf{s}_i\|_2^2 \end{aligned} \tag{5}$$

where $\mathbf{s}_i$ is the dual variable for each constraint i, and ρ is the augmented parameter that enforces the convexity of the function. This problem can be solved by the following iterative scheme:

$$\mathbf{u}_i^{k+1} = \left(\mathbf{H}_i^* \mathbf{H}_i + \rho \mathbf{I}\right)^{-1} \left(\mathbf{H}_i^* \mathbf{g}_i + \rho \left(\mathbf{v}^k - \mathbf{s}_i^k\right)\right) \tag{6}$$

$$\mathbf{v}^{k+1} = \mathbf{S}_{\frac{\lambda}{\rho N}} \left(\bar{\mathbf{u}}^{k+1} + \bar{\mathbf{s}}^k\right) \tag{7}$$

$$\mathbf{s}_i^{k+1} = \mathbf{s}_i^k + \mathbf{u}_i^{k+1} - \mathbf{v}^{k+1} \tag{8}$$

where $\mathbf{S}_\kappa(a)$ is the soft thresholding operator [18] interpreted element wise, defined as follows:

$$\mathbf{S}_\kappa(a) = \begin{cases} a - \kappa \operatorname{sign}(a), & |a| > \kappa \\ 0, & |a| \leq \kappa. \end{cases} \tag{9}$$

$\bar{\mathbf{u}}$ and $\bar{\mathbf{s}}$ are the mean of $\mathbf{u}_i$ and $\mathbf{s}_i$, respectively, for all i. As it can be noticed in (7), the variable $\mathbf{v}$ imposes the consensus, by using all the independent solutions $\mathbf{u}_i$ and $\mathbf{s}_i$. The term

TABLE I
PARAMETERS FOR THE NUMERICAL EXAMPLE

PARAM.	CONFIG.	PARAM.	CONFIG.
λ_c	$4.08 \cdot 10^{-3}$ m	N_p	30000
D	61 λ_c	h_o	0 λ_c
$\langle D^x \rangle = \langle D^y \rangle$	10 λ_c	z_0^T	195 λ_c
D_i^z	$U\,(\mp 0.88\,\lambda_c)$	Δx_0^T	54 λ_c
f	122 λ_c	Δy_0^T	54 λ_c
N_{Tx}	6	Δz_0^T	7.5 λ_c
N_{Rx}	6	l_x	1.08 λ_c
N_f	12	l_y	1.08 λ_c
N_m	432	l_z	1.25 λ_c

$(\mathbf{H}_i^* \mathbf{H}_i + \rho \mathbf{I})^{-1}$ requires the inversion of an $N_p \times N_p$ matrix, which is computationally expensive. However, the *matrix inversion lemma* [19] can be applied in order to perform N inversions of matrices of reduced size $\frac{N_m}{N} \times \frac{N_m}{N}$, as follows

$$\left(\mathbf{H}_i^* \mathbf{H}_i + \rho \mathbf{I}_{N_p}\right)^{-1} = \frac{\mathbf{I}_{N_p}}{\rho} - \frac{\mathbf{H}_i^*}{\rho^2}\left(\mathbf{I}_{\frac{N_m}{N}} + \frac{\mathbf{H}_i \mathbf{H}_i^*}{\rho}\right)^{-1} \mathbf{H}_i \tag{10}$$

where $\mathbf{I}_{N_p}$ and $\mathbf{I}_{\frac{N_m}{N}}$ indicate the identity matrices of sizes N_p and $\frac{N_m}{N}$, respectively.

IV. NUMERICAL RESULTS

The performance of the CRA is evaluated via a mm-wave imaging application. The parameters used for the numerical simulation are shown in Table I. The total number of measurements used for the reconstruction is given by $N_{\mathrm{Tx}} \cdot N_{\mathrm{Rx}} \cdot N_f = 432$. The center frequency of the system is 73.5 GHz, with a bandwidth of 7 GHz. In this example, each scatterer Ω_i is considered as a perfect electric conductor (PEC), so $\sigma_i = \sigma_{\mathrm{PEC}}$. The CRA is discretized into triangular patches, as described in [10]. These triangles are characterized by an averaged size of $\langle D^x \rangle$ and $\langle D^y \rangle$ in $\hat{\mathbf{x}}$ and $\hat{\mathbf{y}}$ dimensions, respectively. The scatterer size D_i^z of each triangle in $\hat{\mathbf{z}}$ is modeled as a uniform random variable. The parameter λ_c is the wavelength at the center frequency. The imaging ROI is located z_0^T away from the focal point of the CRA; and it encloses a volume determined by the following dimensions: Δx_0^T, Δy_0^T, and Δz_0^T in $\hat{\mathbf{x}}$, $\hat{\mathbf{y}}$, and $\hat{\mathbf{z}}$ dimensions. The ROI is discretized into parallelepipeds of side length l_x, l_y, and l_z in $\hat{\mathbf{x}}$, $\hat{\mathbf{y}}$, and $\hat{\mathbf{z}}$ dimensions, respectively.

With the paremeters shown in Table I, the sensing matrix $\mathbf{H}$ has a size of $432 \times 30\,000$. The proposed method divides $\mathbf{H}$ into $N = 24$ submatrices of size $18 \times 30\,000$, which are used for each optimization of $\mathbf{u}_i$. As a result of applying the *matrix inversion lemma*, only 24 matrices of dimension 18×18 need to be inverted instead of one large $30\,000 \times 30\,000$ matrix. The inversion of these 24 matrices is performed just once and used afterward in each iteration, as indicated in (6). The proposed ADMM algorithm highly accelerates the optimization process. Fig. 4 shows the imaging results using: 1) a traditional pseudoinverse approach, where many artifacts appear; 2) constrained NESTA algorithm [8] (tol_var $= 10^{-5}$, $\mu = 0.1$, $\delta = 0.7$); and 3) ADMM, with a norm-1 weight of $\lambda = 10$ and an augmented parameter $\rho = 0.01$, for a structure of four differently shaped targets located among six possible parallel planes. The regularized ADMM solution clearly outperforms the pseudoinverse

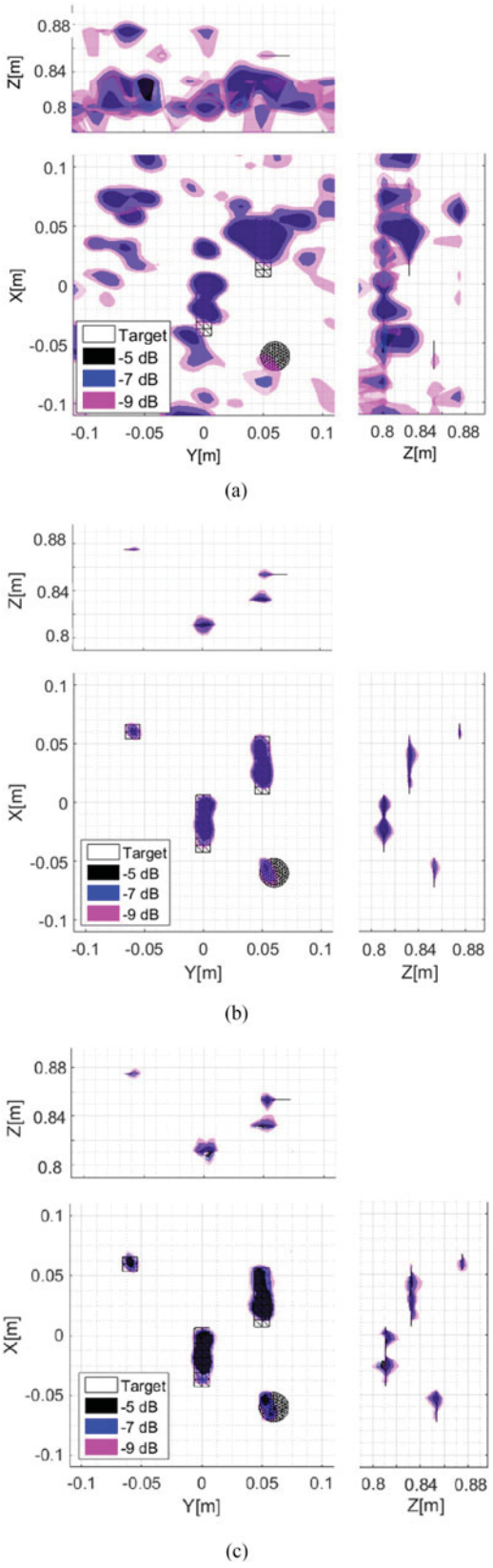

Fig. 4. Imaging reconstruction (top, front, and side views) using (a) pseudoinverse, (b) NESTA, and (c) ADMM. The targets are represented with the transparent black triangles and the reconstructed reflectivity is presented in the colored map.

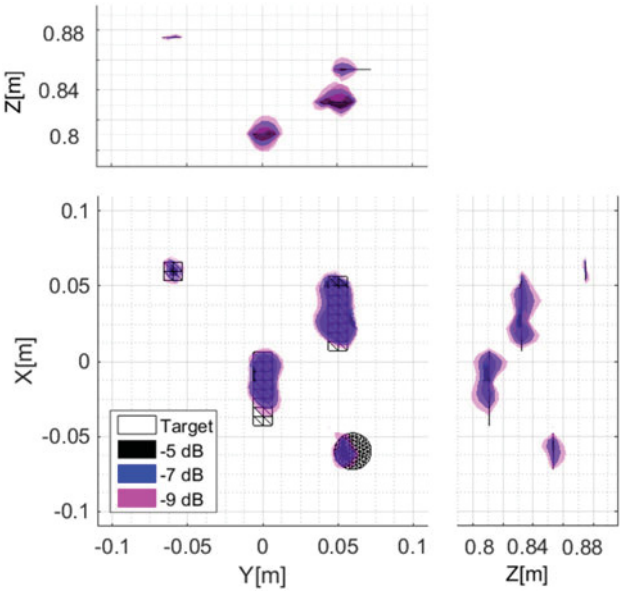

Fig. 5. Imaging reconstruction (top, front, and side views) using ADMM for 50 itearation. The targets are represented with the transparent black triangles, and the reconstructed reflectivity is presented in the colored map.

TABLE II
SIMULATION TIME FOR DIFFERENT ITERATIVE METHODS

Iterative method	Iterations	Time $[s]$
NESTA using CPU	1000	245.7
ADMM using CPU	300	120.8
ADMM using GPU (double precision)	300	5.7
ADMM using GPU (single precision)	300	4.2
ADMM using GPU (single precision)	50	1.0

solution in terms of image quality. Additionally, the ADMM algorithm solved the problem in 121 s for 300 iterations, using a single-threaded M code running on a hexa-core CPU @3.5GHz. In order to show the same image quality, NESTA solves the problem in 246 s for 1000 iterations. (Notice that the number of iterations is independent for each algorithm and cannot be compared.) Since *consensus-based* ADMM algorithm is efficiently parallelizable, it can solve the problem in just 4.2 s running a MATLAB PCT M code using a GTX 1080 GPU (single precision computation), accelerating the computational time more than 96%. Even more, a good image reconstruction can be obtained in just 1 s (50 iteration) with the GPU parallelized ADMM code, as it can be seen in Fig. 5. This speed improvement shows the efficacy of the proposed approach, making real-time imaging possible. Table II shows the time measurements comparison for different methods of performing the norm-1 regularized ADMM solution, compared to NESTA.

V. CONCLUSION

This letter has presented the mathematical principles of a newly distributed, consensus-based, imaging algorithm using the norm-1-regularized ADMM for a CRA. The methodology explanation, the graphical comparison to other techniques, and the convergence process have been explained in this letter. In addition to the simplicity of the proposed algorithm, it outperforms traditional pseudoinverse imaging algorithms in terms of image quality, and current state-of-the-art iterative algorithms (i.e., NESTA) in terms of computational cost. The distributive capabilities of the ADMM for fast imaging, combined with the high sensing capacity of the recently proposed CRA, allow the imaging of metallic targets in a 3-D domain in quasi-real time, with a reduced hardware and a reduced number of measurements.

REFERENCES

[1] J. Martinez Lorenzo, J. Heredia Juesas, and W. Blackwell, "A single-transceiver compressive reflector antenna for high-sensing-capacity imaging," *IEEE Antennas Wireless Propaga. Lett.*, vol. 15, pp. 968–971, 2016.
[2] R. Obermeier and J. A. Martinez-Lorenzo, "Model-based optimization of compressive antennas for high-sensing-capacity applications," *IEEE Antennas Wireless Propagation Lett.*, vol. 16, pp. 1123–1126, 2017.
[3] A. Molaei, J. H. Juesas, G. Allan, and J. Martinez-Lorenzo, "Active imaging using a metamaterial-based compressive reflector antenna," in *Proc. IEEE Int. Symp. Antennas Propag.*, 2016, pp. 1933–1934.
[4] A. Molaei, G. Allan, J. Heredia, W. Blackwell, and J. Martinez-Lorenzo, "Interferometric sounding using a compressive reflector antenna," in *Proc. 10th Eur. Conf. Antennas Propag.*, 2016, pp. 1–4.
[5] H. Gomez-Sousa, O. Rubinos-Lopez, and J. A. Martinez-Lorenzo, "Hematologic characterization and 3D imaging of red blood cells using a compressive nano-antenna and ML-FMA modeling," in *Proc. 10th Eur. Conf. Antennas Propag.*, 2016, pp. 1–5.
[6] G. Oliveri, P. Rocca, and A. Massa, "A Bayesian-compressive-sampling-based inversion for imaging sparse scatterers," *IEEE Trans. Geosci. Remote Sens.*, vol. 49, no. 10, pp. 3993–4006, Oct. 2011.
[7] A. Beck and M. Teboulle, "A fast iterative shrinkage-thresholding algorithm for linear inverse problems," *SIAM J. Imag. Sci.*, vol. 2, no. 1, pp. 183–202, 2009.
[8] S. Becker, J. Bobin, and E. J. Candès, "Nesta: A fast and accurate first-order method for sparse recovery," *SIAM J. Imag. Sci.*, vol. 4, no. 1, pp. 1–39, 2011.
[9] A. Massa, P. Rocca, and G. Oliveri, "Compressive sensing in electromagnetics–A review," *IEEE Antennas Propag. Mag.*, vol. 57, no. 1, pp. 224–238, Feb. 2015.
[10] J. Meana, J. Martinez-Lorenzo, F. Las-Heras, and C. Rappaport, "Wave scattering by dielectric and lossy materials using the modified equivalent current approximation (MECA)," *IEEE Trans. Antennas Propag.*, vol. 58, no. 11, pp. 3757–3761, Nov. 2010.
[11] E. J. Candes, "The restricted isometry property and its implications for compressed sensing," *Comptes Rendus Mathematique*, vol. 346, no. 9/10, pp. 589–592, 2008.
[12] S. Boyd, N. Parikh, E. Chu, B. Peleato, and J. Eckstein, "Distributed optimization and statistical learning via the alternating direction method of multipliers," *Found. Trends Mach. Learn.*, vol. 3, no. 1, pp. 1–122, Jul. 2011.
[13] S. Boyd and L. Vandenberghe, *Convex Optimization*. Cambridge, U.K.: Cambridge Univ. Press, 2009.
[14] M. H. DeGroot, "Reaching a consensus," *J. Amer. Stat. Assoc.*, vol. 69, no. 345, pp. 118–121, 1974.
[15] T. Erseghe, D. Zennaro, E. Dall'Anese, and L. Vangelista, "Fast consensus by the alternating direction multipliers method," *IEEE Trans. Signal Process.*, vol. 59, no. 11, pp. 5523–5537, Nov. 2011.
[16] J. F. Mota, J. Xavier, P. M. Aguiar, and M. Puschel, "Distributed basis pursuit," *IEEE Trans. Signal Process.*, vol. 60, no. 4, pp. 1942–1956, Apr. 2012.
[17] P. A. Forero, A. Cano, and G. B. Giannakis, "Consensus-based distributed support vector machines," *J. Mach. Learn. Res.*, vol. 11, pp. 1663–1707, 2010.
[18] K. Bredies and D. A. Lorenz, "Linear convergence of iterative soft-thresholding," *J. Fourier Anal. Appl.*, vol. 14, no. 5–6, pp. 813–837, Oct. 2008.
[19] M. A. Woodbury, "Inverting modified matrices," *Memorandum Rep.*, vol. 42, p. 106, 1950.